Shallow Slow Earthquake Episodes Near the Trench Axis Off Northern Costa Rica

Satoru Baba[1], Kazushige Obara[1], Shunsuke Takemura[1], Akiko Takeo[1], and Geoffrey A. Abers[2]

[1]Earthquake Research Institute, The University of Tokyo, Tokyo, Japan

[2]Department of Earth and Atmospheric Sciences, Cornell University, Ithaca, New York, United States of America

Corresponding author: Satoru Baba (babasatoru@eri.u-tokyo.ac.jp)

Key Points:

- Shallow very low frequency earthquakes in Costa Rica detected by the matched-filter technique distribute near the trench axis
- Distribution of slow earthquakes complements coseismic slip areas of tsunami and large regular earthquakes
- Similar characteristics of shallow slow earthquakes in Costa Rica and Nankai subduction zones may be due to common tectonic features

Abstract

Slow earthquakes are generally distributed in regions surrounding seismogenic zones along the plate boundaries of subduction zones. In the Costa Rica subduction zone, large regular interplate earthquakes with a magnitude of 7–8 occur repeatedly, and a tsunami earthquake occurred in the northern part in 1992. To clarify the spatial distribution of various slip behaviors at the plate boundary in the Costa Rica subduction zone, we detected and located very low frequency earthquakes (VLFEs) using a grid-search matched-filter technique with synthetic templates based on a regional three-dimensional model. VLFEs were activated in September 2004 and August 2005, and most of the VLFEs were located near the trench axis at a depth range of 5–10 km, the updip of the seismogenic zone. The spatial distribution of VLFEs complements the slip areas of large earthquakes and the tsunami earthquake. Low frequency tremor signals were also found in high-frequency seismogram envelopes within the same time windows of detected VLFEs; thus, we also investigated the energy rates of tremors accompanied by VLFEs. The range of scaled energy, which is the ratio of the seismic energy rate of a tremor to the seismic moment rate of accompanying VLFE, was 10^{-9}–10^{-8}. This value is similar to that in shallow slow earthquakes in the Nankai subduction zone. The similarity of characteristics and distribution of shallow slow earthquakes in the Costa Rica and Nankai subduction zones may be due to common tectonic features, such as age, temperature, or the presence of accretionary prisms.

Plain language summary

Slow earthquakes with slower rupture speeds compared to those of regular earthquakes generally occur on the plate boundaries of subduction zones. We detected and located very low frequency earthquakes (VLFEs), which are a type of slow earthquake, in the Costa Rica subduction zone. VLFEs occurred at a depth range of 5–10 km, and their distribution complements the gap of slip areas of tsunami and large regular earthquakes. Low frequency tremor signals, which are also classified as slow earthquakes, are also found in seismograms of higher frequencies within the same time windows of detected VLFEs. We also estimated the energy rates of tremors accompanied by VLFEs and the range of scaled energy, which relates to the rupture process of seismic phenomena, is 10^{-9}–10^{-8} in Costa Rica. This value is similar to that in shallow slow earthquakes in the Nankai subduction zone. The spatial separation of slow and large regular earthquakes is also common. The similarity in the characteristics of shallow slow earthquakes in both subduction zones may be due to common tectonic features, such as age, temperature, or the presence of accretionary prisms.

1. Introduction

Slow earthquakes are mainly observed in regions surrounding seismogenic zones along the plate boundaries of subduction zones (e.g., Obara & Kato, 2016). Various types of slow earthquakes, such as low frequency tremors (tectonic tremors; e.g., Obara, 2002) or low frequency earthquakes (LFEs; e.g., Shelly et al., 2006), very low frequency earthquakes (VLFEs; e.g., Obara & Ito, 2005), and slow slip events (SSEs; e.g., Dragert et al., 2001) have been observed in many subduction zones. The spatiotemporal correlation of tremors, VLFEs, and SSEs is termed episodic tremor and slip (ETS). ETSs were observed in deep Cascadia (e.g., Rogers & Dragert, 2003; Ghosh et al., 2015) and deep Nankai (e.g., Ito et al., 2007; Obara, 2011), for example. Recently, in the Nankai subduction zone, pore fluid pressure changes are

often observed during tremor and VLFE activities and are considered to reflect shallow SSEs by offshore borehole observations (Araki et al., 2017; Nakano et al., 2018). The hypocenters and focal mechanisms of slow earthquakes are generally consistent with shear slips on the plate boundaries, and the distribution of slow earthquakes is related to large earthquake slip areas, interplate coupling, or fluid distribution (e.g., Baba et al., 2020b; Ghosh et al., 2015; Obara & Kato, 2016).

In the Costa Rica subduction zone, the Cocos plate subducts beneath the Caribbean plate at the Middle America Trench at a rate of approximately 80 mm/year (referred from NUVEL1A; DeMets et al., 1994). In this subduction zone, large thrust-type earthquakes with a moment magnitude (Mw) of 7–8 occur repeatedly (light blue areas in Figure 1a; Protti et al., 1995; Yue et al., 2013). The coseismic slip areas of these large earthquakes were distributed at a depth range of 10–35 km beneath the Nicoya Peninsula and off the coastal area. The latest large earthquake with Mw of 7.6 occurred on 5 September, 2012 (green contour lines in Figure 1a; Yue et al., 2013). In the vicinity of the large thrust earthquake area, a tsunami earthquake with Mw of 7.6 also occurred off Nicaragua located in the north of Costa Rica on 2 September, 1992 (dark blue area in Figure 1a; Satake, 1994).

In addition to large regular and tsunami earthquakes, slow earthquakes also occur in the Costa Rica subduction zone. The Global Navigation Satellite System data revealed that SSEs with Mw of 6.6–7.2 occur at intervals of 21±6 months (Jiang et al., 2012). The large slip area of the SSE in 2007 was separated into the downdip and updip areas of the seismogenic zone (Jiang et al., 2012, 2017; Outerbridge et al., 2010). An SSE preceded the 2012 Mw 7.6 earthquake (Voss et al., 2018), similar to both the slow slip before the 2011 Tohoku earthquake in Japan (Ito et al., 2013; Kato et al., 2012) and the slow slip before the 2014 Iquique earthquake in Chile (Kato & Nakagawa, 2014; Ruiz et al., 2014).

By using high-frequency (>1 Hz) seismograms, Brown et al. (2009) and Outerbridge et al. (2010) located LFEs and tremors in 2007, respectively (Figure 1a). The tremors and LFEs were located in almost the same area, the downdip of the seismogenic zone. Although tremors and LFEs were temporally correlated with the SSE, the location of tremors and LFEs were separated from the large slip area of the 2007 SSE. On the other hand, Walter et al. (2011) located many tremors in the offshore region from 2007 to 2009. Walter et al. (2013) also found that VLFEs appeared in seismograms in a frequency range of 0.02–0.05 Hz and temporally correlated with tremors in the period of the 2008 SSE. Based on beamforming analysis, they suggested that VLFEs also occurred in offshore areas. Due to the limitations of a conventional analysis, the detailed spatial distribution of slow earthquakes in the Costa Rica subduction zone is still not well understood.

The spatial variation of slow and large regular earthquakes can reflect the heterogeneity of the frictional conditions on the plate boundary (e.g., Baba et al., 2020b). To clarify the spatial relationship between slow and large regular earthquake distribution in the Costa Rica subduction zone, an accurate spatial distribution of slow earthquakes is needed. Thus, we detected VLFEs in the Costa Rica subduction zone using a temporary broadband seismic network from August 2004 to January 2006 because signals of VLFEs are less attenuated than those of tremors and propagate longer distances. The method is based on the matched-filter technique. Template waveforms from possible VLFE locations were evaluated by numerical simulations of seismic wave propagation using a regional three-dimensional (3D) velocity structure model. In addition, scaled energy is an informative parameter for the rupture process of seismic phenomena

(Kanamori & Rivera, 2006). By using high-frequency (2–8 Hz) seismograms, we also estimated the seismic energy rate functions of tremors accompanied by VLFEs to evaluate the scaled energy of slow earthquakes in the Costa Rica subduction zone.

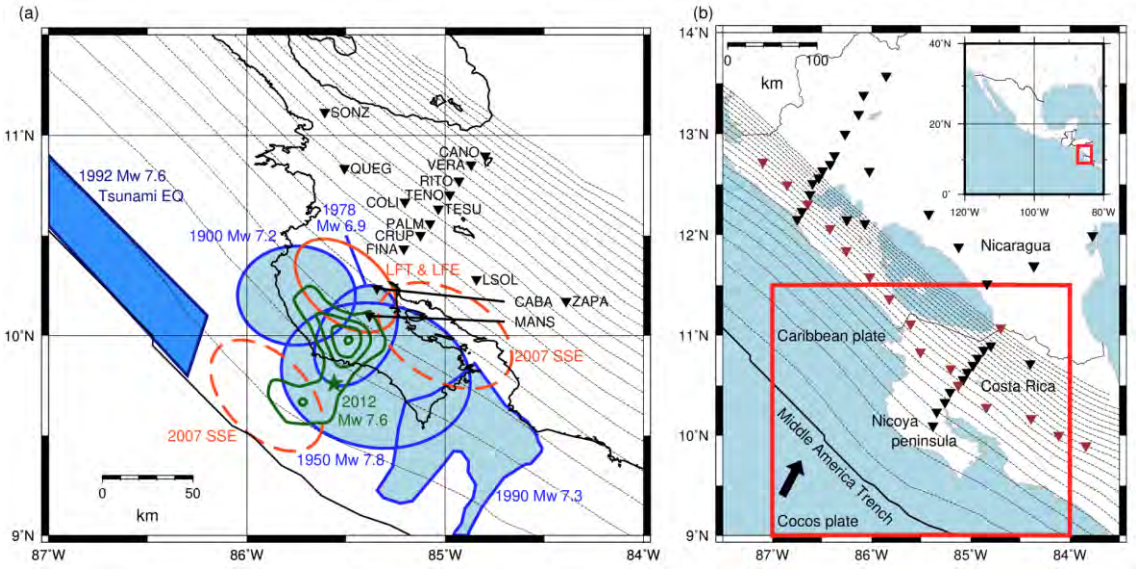

Figure 1. (a) Large regular and slow earthquake areas based on previous studies around Costa Rica. Green contours show the coseismic slip distribution of the 2012 Mw 7.6 earthquake with a 1-m interval (Yue et al., 2013). Blue and dark blue areas show the slip areas of large and tsunami earthquakes (1990 Mw 7.3: Protti et al., 1995; others: Yue et al., 2013). Orange ellipses with dashed lines show large slip areas of the 2007 SSE (Jiang et al., 2017). The orange ellipse with a solid line shows the distributions of LFEs (Brown et al., 2009) and tremors (Outerbridge et al., 2010). Black inverted triangles show the station locations of the TUCAN network used in VLFE detection (Section 2.2). (b) Map of Costa Rica and Nicaragua. Solid line represents the Middle America Trench (slab 2.0; Hayes, 2018). Dashed contours indicate the isodepths of the top of the Cocos Plate with 10 km intervals (slab 2.0; Hayes, 2018). Black arrow indicates the convergence direction of the Cocos Plate, which subducts below the Caribbean plate from the Middle America Trench (NUVEL-1A; DeMets et al., 1994). Inverted triangles show the locations of stations of the TUCAN network. Brown triangles are stations which were used in beamforming (Section 2.3).

2. VLFE analysis

2.1. Data

We used waveforms of a temporary seismic network, Tomography Under Costa Rica and Nicaragua (TUCAN; Abers & Fischer, 2003), recorded from August 2004 to January 2006. There were 49 broadband seismic stations in four lines (Figure 1b). In this study, we mainly used data from stations in Costa Rica (shown in Figure 1a) for VLFE analysis. After removing instrumental responses, the seismograms for VLFE detection were resampled at one sample per second. We applied a bandpass filter in the frequency range of 0.02–0.05 Hz to all the seismograms to enhance the signals of VLFEs.

2.2. Matched-filter technique

The detection procedure used for VLFEs is similar to that used in our previous study (Baba et al., 2020a). We used only the vertical component because the horizontal components of many stations were noisy, and it was difficult to find VLFE signals. We placed 175 virtual source grids on the Cocos Plate boundary at a uniform interval of 0.1° (Figure 2a) and computed synthetic waveforms from these source grids to the stations in Costa Rica using an open-source seismic wave propagation code (OpenSWPC; Maeda et al., 2017). We used a three-dimensional velocity structure model constructed by combining crust 1.0 (Laske et al., 2013), slab 2.0 (Hayes, 2018), and ETOPO1 (Amante & Eakins, 2009), setting the minimum S-wave velocity in the solid columns to 1.0 km/s. We adopted the values of a mean oceanic slab structure (Christensen & Salisbury, 1975) for the physical parameters of the subducting slab (Table S1). For the physical parameters of the other layers except for the slab, we used the values of crust 1.0, and the default parameter set of OpenSWPC. The model covered the region enclosed by the red line (Figure 1b), which was discretized by a uniform grid interval of 0.2 km. The assumed VLFE moment rate function was a Küpper wavelet with a duration of 15 s and an Mw of 4.0 (Figure 4 of Maeda et al., 2017). The focal mechanism at each source grid was assumed to be consistent with the geometry of the plate boundary of slab 2.0 and the plate motion model, NUVEL-1A (DeMets et al., 1994). The time window of each template was set to 150 s from the event origin time. Hereafter, we simply called these synthetic waveforms as template waveforms. Examples of template waveforms at updip and downdip source grids are shown in Figures 2b and 2c, respectively. The signal first arrives at the MANS and the variation of amplitudes is small for the updip source, whereas signals first arriving at the FINA exhibit amplitudes in or near the Nicoya Peninsula that are much larger than in other areas for the downdip source.

We then calculated cross-correlation coefficients (CCs) between the filtered template waveforms and observed seismograms every 1 s. We selected events with station-averaged coefficients larger than a threshold defined as 9.5 times the median absolute deviation of the distributions. In order to decrease false detections by non-VLFE signals, we adopted a strict detection threshold compared to previous studies (e.g., Shelly et al., 2007).

2.3. VLFE location and discarding false detections

Although a strict detection threshold was employed, there are false detections that are caused by other signals, such as local or regional regular earthquakes or teleseismic events. To exclude local or regional earthquakes, we compared the origin time of detected events with a catalog of local and regional regular earthquakes constructed by El Observatorio Vulcanológico y Sismológico de Costa Rica, Universidad Nacional (Catálogo de Temblores de Costa Rica, 2004-2006; Protti, personal comm.). We discarded events whose epicentral distances were less than 150 km and origin times were within ±50 s from the local or regional earthquakes listed in this earthquake catalog. To discard false detections by teleseismic events, we removed the events detected between the *P*-wave arrivals and 600 s after *S*-wave arrivals of teleseismic events (Mw ≥ 5) in the catalog of the United States Geological Survey. The event amplitudes and CCs are positively correlated in general, but events with high amplitudes and low average CCs occasionally appear. These events are considered to be false detections due to teleseismic events absent in the catalogs. Therefore, we did not count events with average CCs below 0.56 and relative amplitudes to templates higher than 0.4. If the relative amplitude to the template was smaller than 0.05, we did not count the event because the signal was too small to judge whether the event is truly existed or not.

For the remaining events, we calculated the variance reduction (VR) between the template and observed waveforms. We estimated VRs using only the vertical components of relatively quiet stations in and around the Nicoya Peninsula (MANS, CABA, FINA, CRUP, and PALM):

$$VR = \left[1 - \frac{\sum_i \int \{f_i(t) - c g_i(t)\}^2 dt}{\sum_i \int \{f_i(t)\}^2 dt}\right] \times 100\% , \quad (1)$$

where $f_i\ (t)$ and $g_i\ (t)$ are the observed and template waveforms at the i-th station, respectively, and c is the relative amplitude of the observed waveform to the template. We selected events whose VRs were larger than 30%. This threshold is set by trial and error based on visual identifications of VLFEs in the observed data.

After the above procedures, falsely detected events still remained because we only used the vertical component and the array configuration was cross shaped. To discard the remaining false detections, we estimated the normalized-and-stacked amplitude, azimuth, and velocity of signal propagation by applying delay-and-sum beamforming (Section 3.1 of Rost and Thomas, 2002; Walter et al. 2013) to vertical component seismograms. After normalizing the waveform of each station by its maximum amplitude in the 150 s time window, we searched for the azimuth and velocity that maximized the stacked amplitude by performing a grid search for the azimuth between 135º – 315º with 1º intervals and the velocity between 2–5 km/s with 0.1 km/s intervals. We first used the along-strike stations in both Costa Rica and Nicaragua (brown inverted triangles in Figure 1b) to discard teleseismic events. The amplitudes of Costa Rican VLFEs in the Nicaraguan station are generally very small compared with those in the Costa Rican stations. Therfore, we selected the event whose stacked amplitude normalized by the number of stations was smaller than 0.6 because events with large stacked signals are suspected as teleseismic earthquakes. We then conducted another beamforming analysis for the remaining events using the same stations as the matched-filter analysis, and selected events whose azimuth was 200–230º. Finally, to avoid duplicate detection, we detected a VLFE with a maximum CC every 60 s from the remaining VLFE candidates.

2.4. Estimation of the moments of events

We estimated the source durations of detected VLFEs by comparing template waveforms with durations of 10–50 s and an Mw of 4.0 with observed waveforms (like Yabe et al., 2020). The duration that resulted in the highest values of CC between the observed and template waveforms was adopted.

We also calculated the relative amplitude of an event to template waveforms with source durations of the highest CC and an Mw of 4.0 using the same method as Baba et al. (2020b). The relative amplitude can be used to calculate the seismic moments of each VLFE. The seismic moment rate of a VLFE was calculated by dividing its seismic moment by its duration.

2.5. Characteristics of detected VLFEs

We detected 68 VLFEs during the analysis period. Example traces of a VLFE located at 85.8°W and 9.4°N are shown in Figure3, and the signal of this VLFE first arrives at the MANS and propagates to inland stations (top panel of Figure 3). This feature was confirmed in the case of the updip templates (Fig. 2b). There is a tremor signal in the frequency range of 2–8 Hz in the same time window (middle and bottom panels of Figure 3). The cumulative number of VLFEs showed significant increases in September 2004 and August 2005 (Figure 4a). In August 2005,

an SSE was reported by Jiang et al. (2012); therefore, SSE and VLFE activities were temporally correlated.

Most of the VLFEs (64 events) are distributed at a depth range of 5–10 km, near the trench axis (Figure 4b), at the updip of the seismogenic zone. The area overlaps with the shallower part of the large slip area of the 2007 SSE (Jiang et al., 2017). Although the slip distribution of the 2005 SSE was not estimated in previous studies, our results suggest that the 2005 SSE can also have a large slip area near the trench axis, similar to the 2007 SSE. The distribution of VLFEs complements the gap of large slip areas of thrust-type large interplate earthquakes with an Mw of 7–8 in Costa Rica and the 1992 tsunami earthquake with an Mw of 7.6. The depth range and the separate distribution between VLFEs and large earthquakes are similar to shallow slow earthquakes in the Nankai subduction zone.

The distribution of the CC confirms that most of the VLFEs were located near the trench axis. CCs for more than half of the events exceeded the threshold only in the updip (Figure 5a). For several events, CCs exceeded the threshold both in the updip and downdip of the seismogenic zone with a larger CC in the updip (Figures 5b). On the other hand, 5 VLFEs were located at a depth of ~40 km at the downdip of large earthquakes (Figure 4b). However, we cannot exclude the possibility that such VLFEs occur in the updip in real because, in such cases, two CC peaks tend to appear both in the updip and downdip (Figure 5c). Of course, there is a possibility that such VLFEs really occur in the downdip because the locations of such VLFEs were near the locations of previously reported LFEs (Brown et al. 2009) and tremors (Outerbridge et al. 2010). In this study, the SN ratios of VLFEs detected in the downdip are very low; hence, it is difficult to judge whether such VLFEs occur in downdip or updip. The reason for the small number and the low SN ratio of downdip events may be that slow earthquakes in the downdip were inactive during 1.5 years of the temporary observation. To investigate whether deep VLFEs really exist, an analysis with a longer dataset is needed in future work.

The Mw and duration of VLFEs were mainly distributed in 3.4–4.2 and 10–30 s, respectively (Figures 6a, b). The Mw and duration of VLFEs have a positive correlation (Figure 6c) as with shallow VLFEs in Nankai, Japan (Sugioka et al., 2012; Takemura et al., 2019). Although the lower limit of Mw is large (~3.4) due to a strict threshold, the distribution of Mw and duration of VLFEs in Costa Rica is similar to that of shallow VLFEs in Nankai.

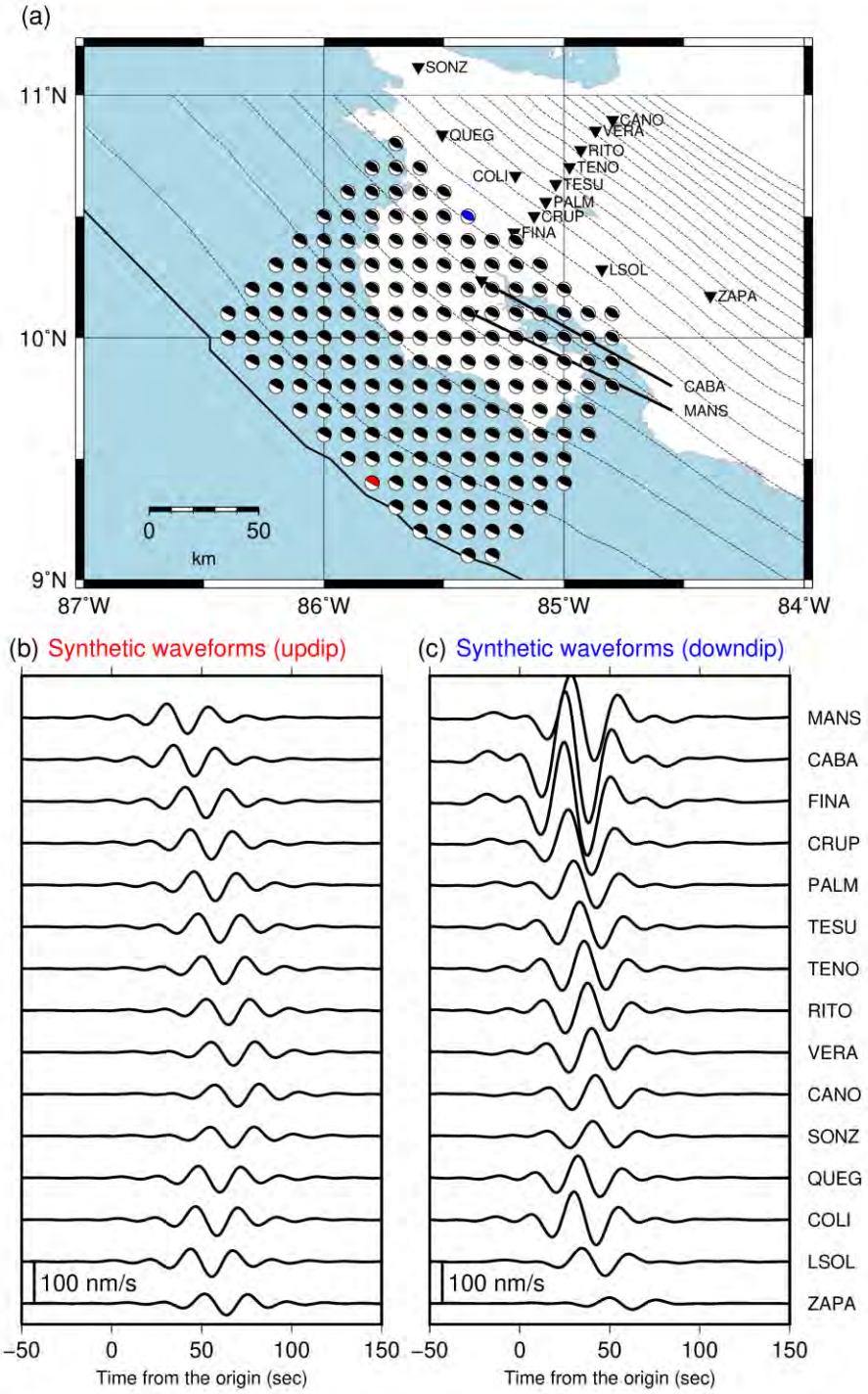

Figure 2. (a) Virtual source grids assumed in this study. Beach balls show the locations and focal mechanisms of the virtual sources. Inverted triangles, the black line, and dashed contours are the same as in Figure 1. Examples of waveforms of virtual sources in the (b) updip and (c) downdip areas. Sources of Figures 1b and 1c are shown by the red and blue beachballs in Figure 2a, respectively.

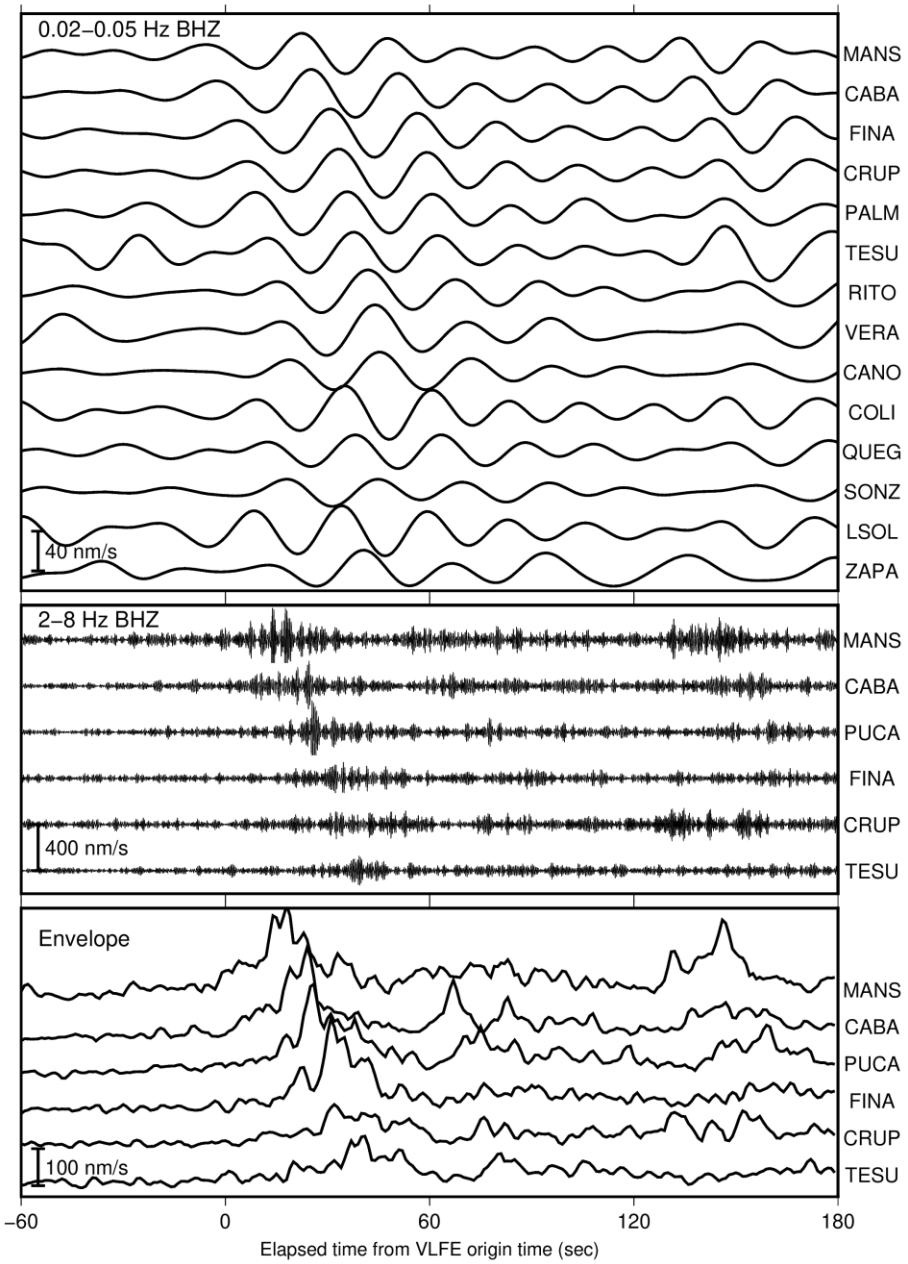

258

259 **Figure 3.** Example of waveforms of a VLFE and the corresponding tremor located at 85.8°W
260 and 9.4°N (shown by a red beachball in Figure 2a) in the frequency range of 0.02–0.05 Hz and
261 2–8 Hz, and smoothed root-mean-square envelope in the frequency range of 2–8 Hz.
262 Seismograms are shown from the origin time of the VLFE, 03:53:47 (UTC), August 10, 2012.

263

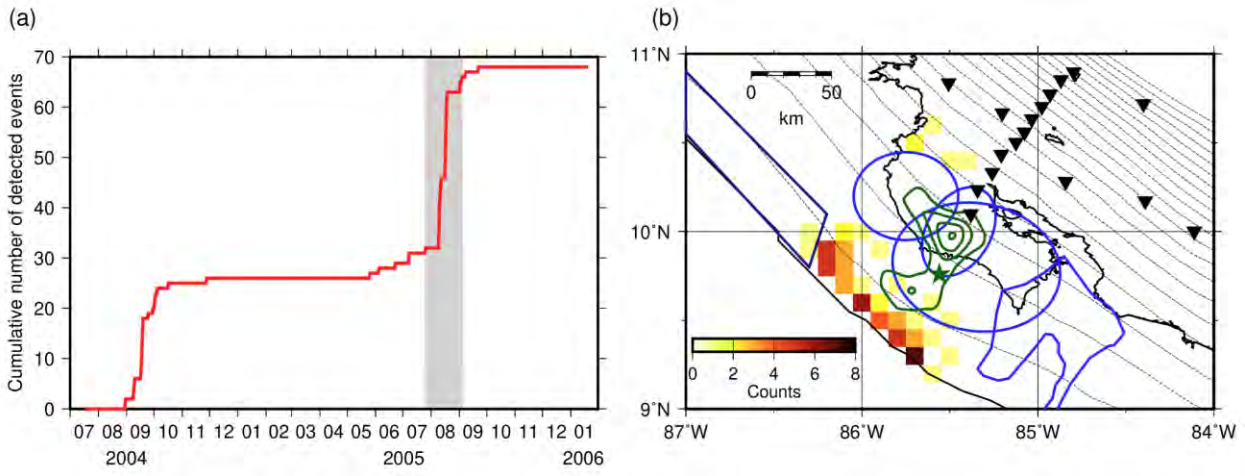

Figure 4. (a) Cumulative number of the VLFEs from July 2004 to January 2006. Gray shading shows the period of the 2005 SSE (Jiang et al., 2012). (b) Distribution of the number of detected events at each virtual source. Blue ellipses and polygons, dark blue quadrangle, inverted triangles, black line, and dashed contours are the same as in Figure 1.

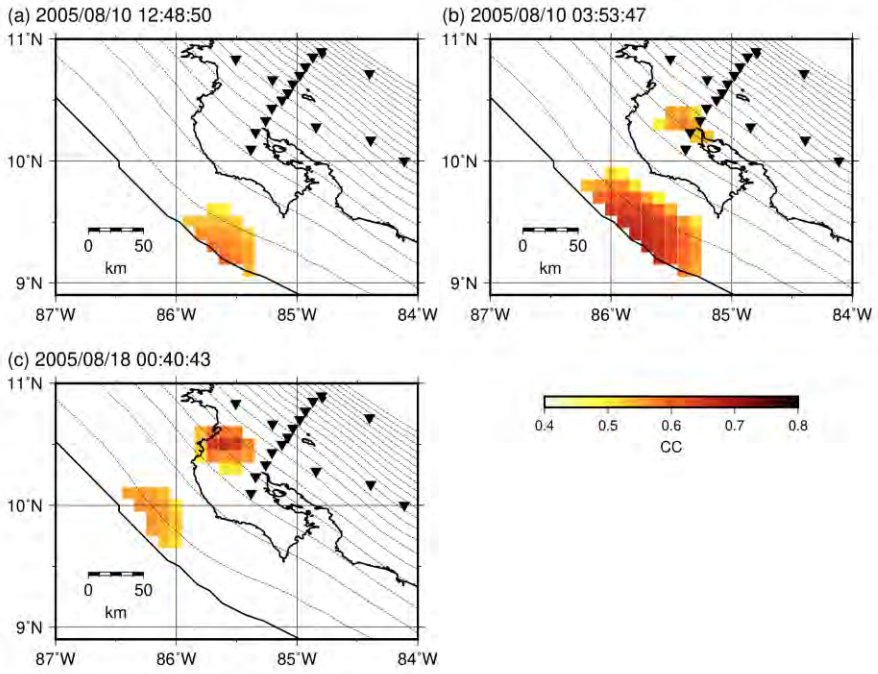

Figure 5. Examples of CC distributions of (a) an event which has large CCs only in updip grids, (b) an event which has large CCs both in updip and downdip grids but is located in an updip grid, and (c) an event which has large CCs both in updip and downdip grids but is located in a downdip grid. Inverted triangles, black line, and dashed contours are the same as in Figure 1.

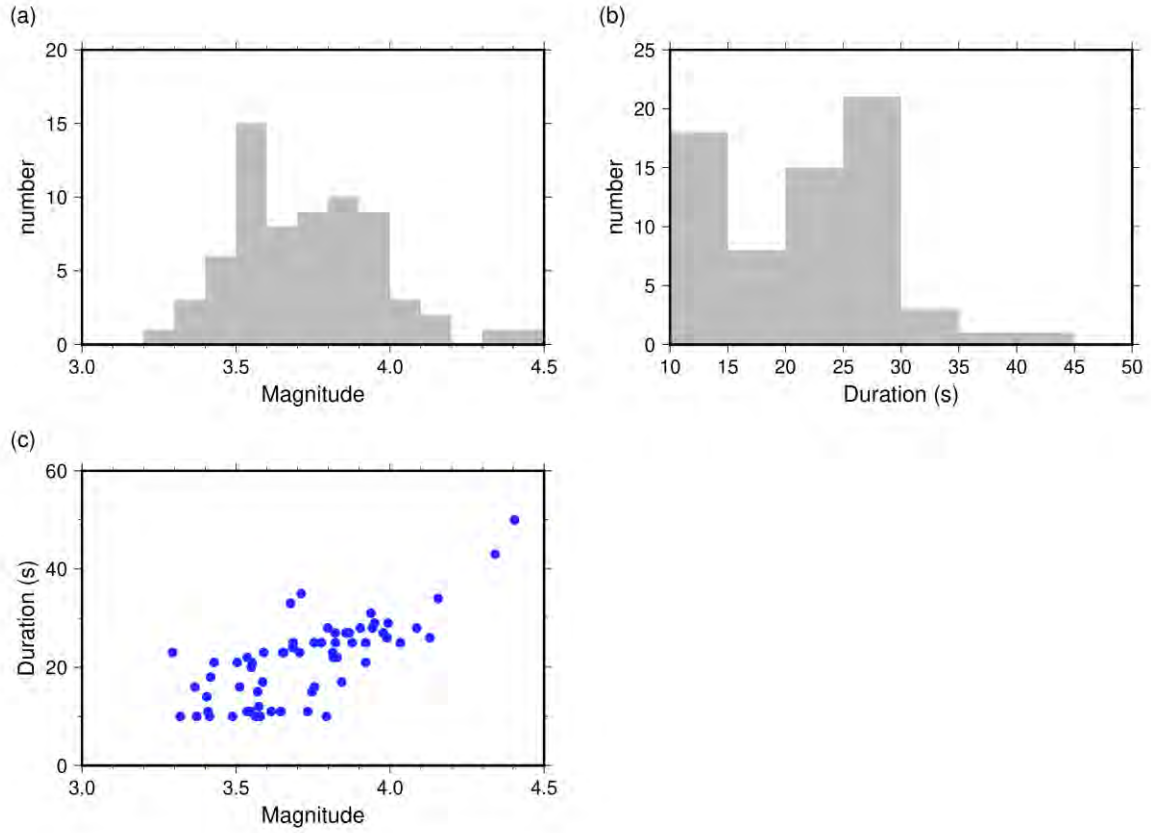

Figure 6. Distribution of (a) magnitudes and (b) durations of VLFEs. (c) Relationship between durations and magnitudes of VLFEs.

3. Estimations of seismic energy rates for tremors accompanied by VLFEs

Tremor signals were also found in the frequency range of 2–8 Hz within the same time windows of detected VLFEs (middle panel of Figure 3). It is difficult to locate tremors in the offshore region by using an onshore network because sources of tremors are distant from the network and signals of tremors attenuate strongly compared to VLFE (0.02–0.05 Hz) signals. Based on the spatiotemporal correlation between VLFEs and tremors reported in other regions (e.g., Ghosh et al., 2015; Maeda & Obara, 2009; Tamaribuchi et al., 2019), we estimated the energy rate functions of tremors accompanied by VLFEs by assuming that a tremor occurs at the same location as the VLFE.

We also used waveforms of the TUCAN network similarly to the VLFE detection. After applying a bandpass filter of 2–8 Hz, the envelope waveforms were calculated by taking the root-mean-square of sums of three-component squared seismograms and a smoothing time window of 3 s (bottom panel of Figure 3). The envelope waveforms were resampled at one sample per second.

3.1. Quality factor of the apparent *S*-wave attenuation

To estimate the energy rate functions of tremors accurately, we estimated the quality factor of the apparent *S*-wave attenuation ($Q_{app.}$), based on the coda-normalization method (e.g.,

Aki, 1980; Yoshimoto et al., 1993). First, we selected some isolated regular earthquakes (Figure S1). To eliminate the effect of differences in source size and site amplification, observed maximum *S*-wave amplitudes were normalized by averaged coda amplitudes within a lapse time of 80-90 s. The coda-normalized maximum *S*-wave amplitude of the *i*-th earthquake at the *j*-th station (A_{ij}) and the distance between the hypocenter of the *i*-th earthquake and *j*-th station (L_{ij}) have the following relationship (Takemura et al., 2017):

$$\ln\left(L_{ij}A_{ij}\right) = -\frac{\pi f_c Q_{app.}^{-1}}{V_s} L_{ij} + C' \ , \quad (2)$$

where V_s is the *S*-wave velocity (assuming 3.5 km/s in this study), f_c is the central frequency (assuming 5 Hz in this study), and *C'* is a constant. By solving Equation (2) by the least-squares method, we estimated $Q_{app.}^{-1}$ as $10^{-2.42}$ (Figure 7a).

3.2. Site amplification factor

We estimated the site amplification factor at 2–8 Hz using relative coda amplitudes (e.g., Maeda and Obara, 2009). Coda amplitudes at a certain time window generally depend on the source size and site amplification (e.g., Chapters 2 and 3 of Sato et al., 2012). Therefore, the ratio of the coda wave amplitude at a station to that at a reference station for the same event depends only on the site amplification factor relative to a reference station.

We calculated the ratios of the coda amplitudes for each station to those of the MANS (reference station) for each regular earthquake used in Section 3.1. The time window for evaluating relative coda amplitudes is the same as that in coda-normalization in Section 3.1. Then we calculated the average of the coda amplitude ratios of all earthquakes for each station. The estimated relative site amplification factors at each station used in the estimations of the energy rate functions of tremors are shown in Figure 7b. We compared coda amplitudes of regular earthquakes at the MANS with those at the JTS, a permanent station of the Global Seismograph Network by Incorporated Research Institutions for Seismology and International Deployment of Accelerometers (Scripps Institution of Oceanography, 1986). The average ratio of coda amplitudes at MANS to those at JTS is 1.14, suggesting that the condition of the MNAS site is very similar to that of the JTS.

3.3. Seismic energy rate of tremors

By using apparent attenuation ($Q_{app.}^{-1}$) and site amplification in the previous subsections, we estimated the energy rate functions of tremors. The source energy rate function of a tremor ($E_j\ (t)$) using the amplitude of the *j*-th station is calculated by the following formula (Maeda & Obara, 2009):

$$E_j(t) = 2\pi V_S r_j^2 \rho A'^2_j(\mathrm{t} + t_j)\exp(2\pi f_c Q_{app.}^{-1} t_j) \ , \quad (3)$$

where $A'_j\ (t)$ is the site-corrected amplitude of the envelope waveform of the *j*-th station, r_j is the hypocentral distance from the accompanying VLFE, t_j is the travel time from the VLFE source, and ρ is the density (assuming 2,700 kg/m^3). For calculating $E_j\ (t)$, we used a 180 s time window that started 60 s before the origin time of VLFEs. We calculated the CCs of all station pairs in Figure 7b. To estimate the source energy rate function of the tremor, we only used stations whose CCs with at least one other station exceeded 0.6.

The seismic energy rate W_j using the amplitude of the *j*-th station is given by the integration of the source energy rate function $E_j\ (t)$ in time:

$$W_j = \frac{1}{t_2 - t_1} \int_{t_1}^{t_2} E_j(t)dt \ , \quad (4)$$

where t_1 and t_2 are the start and end of the integration range, respectively. The integration range is defined as the period in which the values of $E_j\ (t)$ exceeded 20% of the maximum value of $E_j\ (t)$ (Figure 8). The seismic energy rate of a tremor (W_0) was obtained by calculating the average W_j of all stations. The error of W_0 was obtained by calculating the standard deviation of W_j.

The energy rates of tremors were mainly distributed in 10^3–$10^{5.5}$ J/s (Figure 9). There is a positive correlation between the energy rates of tremors and the moment rates of the corresponding VLFEs. We estimated the scaled energy by calculating the ratio between the seismic energy rate of a tremor and the seismic moment rate of the corresponding VLFE. The scaled energy of slow earthquakes in the Costa Rica subduction zone is mainly distributed in the range of 10^{-9}–10^{-8} (dotted lines in Figure 9).

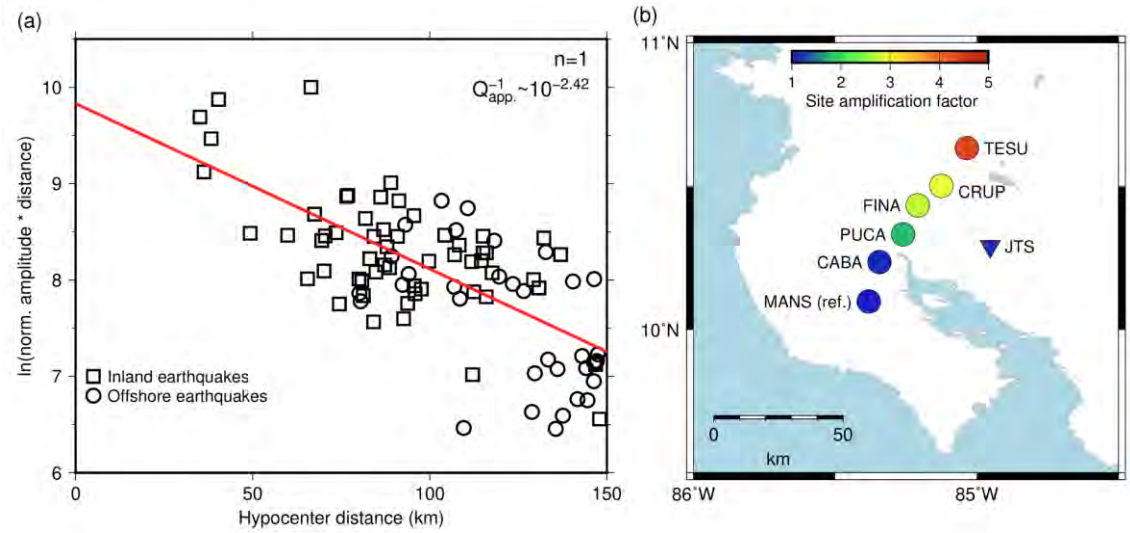

Figure 7. (a) Relationship between logarithm of coda-normalized maximum *S*-wave amplitudes and hypocentral distances. To eliminate effects of geometrical spreading of *S*-wave, coda-nomadized *S*-wave amplitudes were multiplied by their hypocentral distance. Red line shows the regression line using Equation (2). (b) Site amplification factors relative to the MANS based on relative coda amplitude measurements.

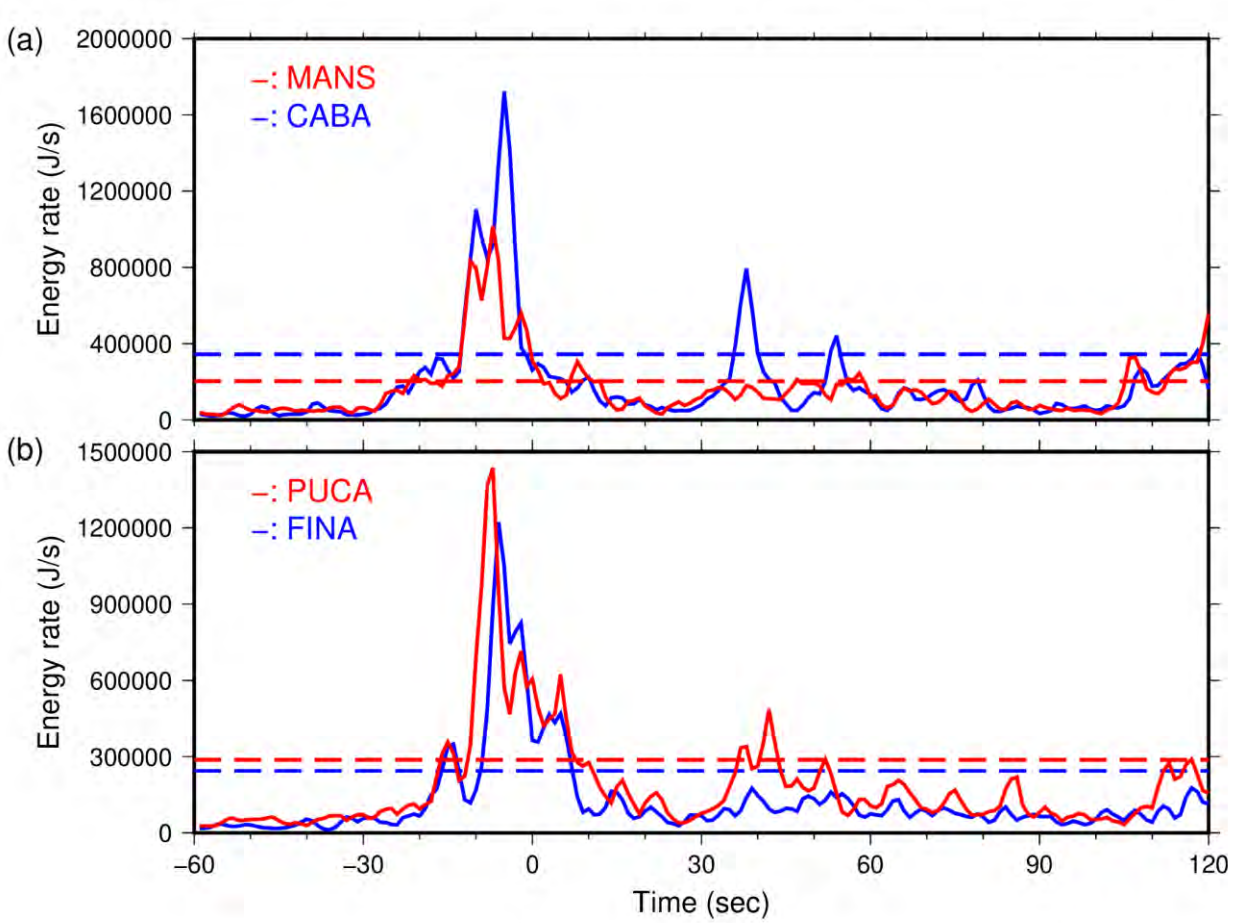

355

356 **Figure 8.** Temporal changes of energy rate functions of a tremor in (a) MANS and CABA and
357 (b) PUCA and FINA. The corresponding VLFE occurs on 03:53:47 (UTC), August 10, 2012.
358 Dashed lines indicate the threshold, which is set as 20% of the maximum value of the energy rate
359 functions.

360

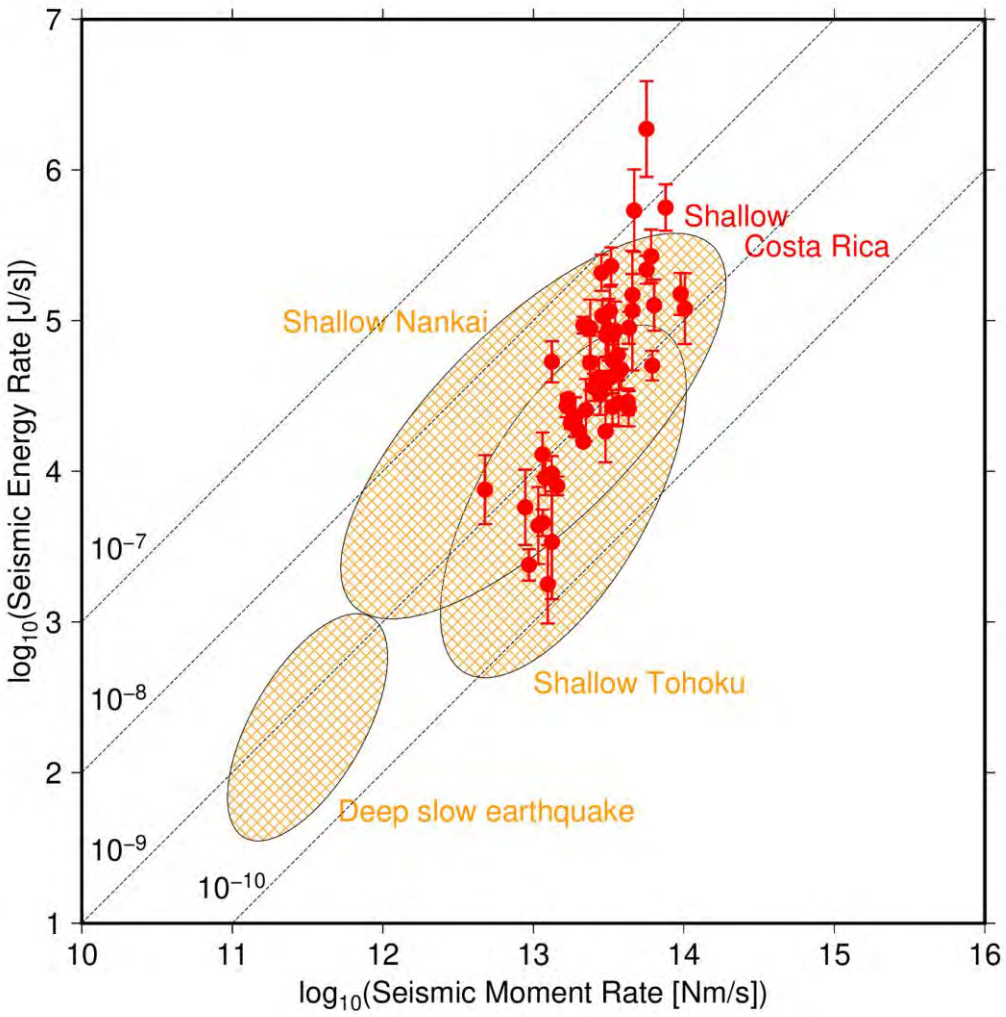

Figure 9. Relationship between seismic moment rates of VLFEs and seismic moment rates of tremors estimated in this study. Dashed lines show scaled energies of 10^{-7}, 10^{-8}, 10^{-9}, and 10^{-10}. Orange shadings show the distributions of shallow slow earthquakes in the Nankai (Yabe et al., 2019) and Tohoku subduction zones (Yabe et al., 2020), and deep slow earthquakes in southwest Japan (Ide & Yabe, 2014), Cascadia (Ide, 2016) and Mexico (Ide & Maury, 2018).

4. Discussion

4.1. shallow ETS in the Costa Rica subduction zone

The activation of VLFEs and tremors in August 2005 temporally correlates with the 2005 SSE reported by Jiang et al. (2012). VLFEs and tremors occurred mainly in the updip area in August 2005; hence, the slip area of the 2005 SSE can be distributed in the updip area near the trench axis, similar to the 2007 SSE. In areas where shallow VLFEs occurred, subseafloor hydrological observatories were installed and pore fluid pressure transients were recorded in 2000 (Brown et al., 2005), 2003–2004 (Solomon et al., 2009), and 2007–2013 (Davis et al., 2011; 2015). They interpreted that pore fluid pressure transients were caused by SSEs. Spatial correspondence of pore fluid change and VLFE activity near the trench in Costa Rica suggests

the occurrence of a shallow ETS, as with the Nankai subduction zone (Araki et al., 2017; Nakano et al., 2018).

4.2. Separation of slow earthquakes and other phenomena

Before the 2012 Mw 7.6 earthquake, the interplate coupling of the shallow slow earthquake area at a depth range of 5–10 km was expected to be very weak (Feng et al., 2012), whereas the coseismic slip area of the earthquake was strongly coupled (Protti et al., 2014). The average stress drop of small-to-moderate regular earthquakes inside the large slip area of the 1992 tsunami earthquake (surrounded by dark blue lines in Figure 4) was 1.2 MPa, which was smaller than that outside the large slip area (Bilek et al., 2016). The values of reported stress drops of slow earthquakes in the Nankai subduction zone were 0.1–200 kPa (e.g., Ito & Obara, 2006; Takagi et al., 2019), which is much smaller than those of regular and tsunami earthquakes. The spatial variation of interplate coupling and stress drop of slips at the plate boundary indicates the heterogeneous distribution of frictional properties at the plate boundary in the Costa Rica subduction zone. In addition, a low stress drop suggests a high pore pressure generated by the existence of fluids (Yao & Yang, 2020). Therefore, the frictional strength of the slow earthquake area at a depth range of 5–10 km can be quite weak owing to the rich fluid compared to that in the regions with regular and tsunami earthquakes.

In the Costa Rica subduction zone, repeating earthquakes were activated after the 2012 Mw 7.6 earthquake around the large coseismic slip area of the earthquake (Chaves et al., 2020). Such activation after a large earthquake in the afterslip area was also observed in the Tohoku subduction zone (Uchida & Matsuzawa, 2013). The locations of repeating earthquakes separate from the areas where VLFEs occur. Such separation is also found in the Nankai (e.g., Takemura et al., 2020) and the Tohoku subduction zone (e.g., Nishikawa et al., 2019).

4.3. Comparison with other subduction zones

Our study revealed that shallow slow earthquakes in the Costa Rica subduction zone occur near the trench axis, in the updip of coseismic slip areas of thrust-type large earthquakes with an Mw of 7–8. The spatial relationship between large and shallow slow earthquakes is common to the Nankai subduction zone.

There are other common features in shallow slow earthquakes between the Costa Rica and Nankai subduction zones. The ranges of magnitudes and durations of shallow VLFEs in the Costa Rica subduction zone are also similar to those in the Nankai subduction zones (e.g., Takemura et al., 2019). The recurrence intervals of activations of slow earthquakes are one to several years in Costa Rica (Jiang et al., 2012), which is similar to shallow slow earthquakes in the Nankai subduction zone, compared to the shorter intervals of deep slow earthquakes in Nankai (e.g., Baba et al., 2020b). Although the number of tremors whose energy rates are less than 10^4 J/s is small because of the strict detection threshold of the corresponding VLFEs, the upper limit of the energy rate range of tremors is similar to that of shallow tremors in Nankai (Yabe et al., 2019). The estimated scaled energy of slow earthquakes in Costa Rica is also similar to that of shallow slow earthquakes in the Nankai subduction zone (Yabe et al., 2019). These results suggest that the characteristics of frictional properties within shallow slow earthquake areas are similar in both the Costa Rica and Nankai subduction zones. On the other hand, the scaled energy range is 0.5–1 orders of magnitude larger than that of shallow slow earthquakes in the Tohoku subduction zone (Yabe et al., 2020), and approximately 1 order of

magnitude larger than that of deep slow earthquakes in Nankai (Ide et al., 2008; Maeda & Obara, 2009).

The shallower parts of Costa Rica and Nankai subduction zones have some common tectonic features. The ages of both subduction zones are similar (15–20 Ma; Syracuse et al., 2010), and they are relatively warm subduction zones (Syracuse et al., 2010) and have thick low-velocity accretionary prisms (Costa Rica: Shipley et al., 1990; Nankai: Tonegawa et al., 2017). The similarity of scaled energy and distribution of slow earthquakes in both subduction zones may be due to similar tectonic environments.

In previous studies, the large slip area of the SSE in 2007 was separated into deeper and shallower parts (Jiang et al., 2017), and deep LFEs and tremors were detected in the downdip area of the seismogenic zone (Brown et al., 2009; Outerbridge et al., 2010). If these events occur in the downdip area, slow earthquakes might occur at separate depths of both shallower and deeper extensions of rupture zones of large earthquakes (Figure 10). This characteristic might also be the same as that of the Nankai subduction zone (Obara & Kato, 2016).

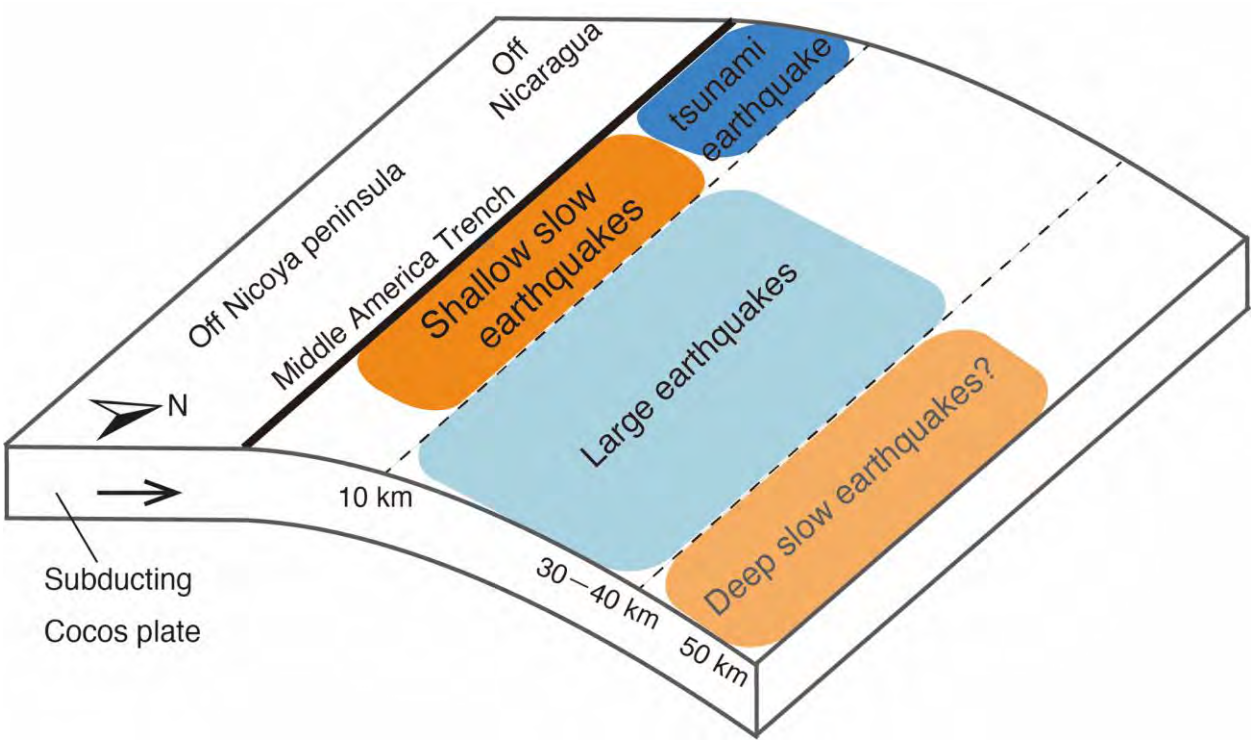

Figure 10. A schematic illustration showing the interpretation of distributions of slow, tsunami, and large regular earthquakes in the Costa Rica subduction zone. The areas of large earthquakes, the 1992 tsunami earthquake, and deep slow earthquakes are referred from Yue et al. (2013), Satake (1994), and Outerbridge et al. (2010), respectively.

5. Conclusions

Based on the grid-search matched-filter technique using synthetic templates in the regional 3D model, we detected and located VLFEs in the Costa Rica subduction zone. Many VLFEs occurred in September 2004 and August 2005, and most of the VLFEs were located near the trench axis, at a depth range of 5–10 km, in the updip of the seismogenic zone. The region

with VLFE activity overlaps with the shallower part of the large slip area of the 2007 SSE; therefore, the occurrences of shallow SSEs are suggested in September 2004 and August 2005. The distribution of VLFEs complements the gap in coseismic slip areas of tsunami and large regular earthquakes. This separation reflects the spatial distribution of the frictional strength of the plate boundary in the Costa Rica subduction zone.

By using high-frequency seismogram envelopes, we also estimated the energy rates of tremors accompanying VLFEs. The ranges of magnitude and duration of VLFEs, energy rate of tremors, and scaled energy in Costa Rica are similar to those in shallow slow earthquakes in the Nankai subduction zone. The similarity of these ranges and the distribution of slow earthquakes in both subduction zones may be due to common tectonic features, such as age, temperature, or the presence of accretionary prisms.

Data Availability

We used seismograms of the TUCAN network (Abers & Fischer, 2003; https://doi.org/10.7914/SN/YO_2003) and Global Seismograph Network (Scripps Institution of Oceanography, 1986; https://doi.org/10.7914/SN/II). We used the earthquake catalog of the U.S. Geological Survey (https://earthquake.usgs.gov/earthquakes/search/). We used OpenSWPC code Version 5.0.2 (Maeda et al., 2017; https://doi.org/10.5281/zenodo.3712650) for the numerical simulations. Numerical simulations were conducted using the Fujitsu PRIMERGY CX600M1/CX1640M1 (Oakforest-PACS) at the Information Technology Center, the University of Tokyo. We used generic mapping tools (Wessel et al., 2013) and Seismic Analysis Code (Helfrich et al., 2013) to prepare the figures and process seismograms, respectively. The VLFE and tremor catalog constructed by this study is provided in an open access repository, zenodo (doi: 10.5281/zenodo.4072375).

Acknowledgements

We would like to thank Suguru Yabe for valuable discussions. We would alsi like to thank Marino Protti for providing the earthquake catalog in Costa Rica and for discussions. We thank Editage (www.editage.com) for English proofreading. This research was supported by JSPS KAKENHI Grant in Science Research on Innovative Areas “Science of Slow Earthquakes” (JP16H06473) and JSPS Research Fellowship DC1 (JP19J20760). This study was also supported by the ERI-JURP 2020-S-04.

References

Abers, G. A., & Fischer, K. M. (2003). Tomography Under Costa Rica and Nicaragua. International Federation of Digital Seismograph Networks. https://doi.org/10.7914/SN/YO_2003

Aki, K. (1980). Attenuation of shear-waves in the lithosphere for frequencies from 0.05 to 25 Hz. *Physics of the Earth and Planetary Interiors*, *21*(1), 50–60. https://doi.org/10.1016/0031-9201(80)90019-9

Amante, C., & Eakins, B.W. (2009). ETOPO1 1 Arc-Minute Global Relief Model: Procedures, Data Sources and Analysis. NOAA Technical Memorandum NESDIS NGDC-24. https://doi.org/10.7289/V5C8276M

Araki, E., Saffer, D. M., Kopf, A. J., Wallace, L. M., Kimura, T., Machida, Y., et al. (2017). Recurring and triggered slow-slip events near the trench at the Nankai Trough subduction megathrust. *Science*, *356*(6343), 1157–1160. https://doi.org/10.1126/science.aan3120

Baba, S., Takeo, A., Obara, K., Matsuzawa, T., & Maeda, T. (2020a). Comprehensive Detection of Very Low Frequency Earthquakes Off the Hokkaido and Tohoku Pacific Coasts, Northeastern Japan. *Journal of Geophysical Research: Solid Earth*, *125*(1), 1–13. https://doi.org/10.1029/2019JB017988

Baba, S., Takemura, S., Obara, K., & Noda, A. (2020b). Slow Earthquakes Illuminating Interplate Coupling Heterogeneities in Subduction Zones. *Geophysical Research Letters*, *47*(14), 4–5. https://doi.org/10.1029/2020GL088089

Bilek, S. L., Rotman, H. M. M., & Phillips, W. S. (2016). Low stress drop earthquakes in the rupture zone of the 1992 Nicaragua tsunami earthquake. *Geophysical Research Letters*, *43*(19), 10,180-10,188. https://doi.org/10.1002/2016GL070409

Brown, J. R., Beroza, G. C., Ide, S., Ohta, K., Shelly, D. R., Schwartz, S. Y., et al. (2009). Deep low-frequency earthquakes in tremor localize to the plate interface in multiple subduction zones. *Geophysical Research Letters*, *36*(19), 1–5. https://doi.org/10.1029/2009GL040027

Brown, K. M., Tryon, M. D., DeShon, H. R., Dorman, L. R. M., & Schwartz, S. Y. (2005). Correlated transient fluid pulsing and seismic tremor in the Costa Rica subduction zone. *Earth and Planetary Science Letters*, *238*(1–2), 189–203. https://doi.org/10.1016/j.epsl.2005.06.055

Chaves, E. J., Schwartz, S. Y., & Abercrombie, R. E. (2020). Repeating earthquakes record fault weakening and healing in areas of megathrust postseismic slip, 2–10.

Christensen, N. I., & Salisbury, M. H. (1975). Structure and constitution of the lower oceanic crust. *Reviews of Geophysics*, *13*(1), 57–86. https://doi.org/10.1029/RG013i001p00057

Davis, E., Heesemann, M., & Wang, K. (2011). Evidence for episodic aseismic slip across the subduction seismogenic zone off Costa Rica: CORK borehole pressure observations at the subduction prism toe. *Earth and Planetary Science Letters*, *306*(3–4), 299–305. https://doi.org/10.1016/j.epsl.2011.04.017

Davis, E. E., Villinger, H., & Sun, T. (2015). Slow and delayed deformation and uplift of the outermost subduction prism following ETS and seismogenic slip events beneath Nicoya Peninsula, Costa Rica. *Earth and Planetary Science Letters*, *410*, 117–127. https://doi.org/10.1016/j.epsl.2014.11.015

DeMets, C., Gordon, R. G., Argus, D. F., & Stein, S. (1994). Effect of recent revisions to the geomagnetic reversal time scale on estimates of current plate motions. *Geophysical Research Letters*, *21*(20), 2191–2194. https://doi.org/10.1029/94GL02118

Dragert, H., Wang, K., & James, T.S. (2001) A silent slip event on the deeper Cascadia subduction interface. *Science*, 292, 1525–1528. https://doi.org/10.1126/science.1060152

Feng, L., Newman, A. V., Protti, M., Gonzlez, V., Jiang, Y., & Dixon, T. H. (2012). Active deformation near the Nicoya Peninsula, northwestern Costa Rica, between 1996 and 2010: Interseismic megathrust coupling. *Journal of Geophysical Research: Solid Earth*, *117*(6), 1–23. https://doi.org/10.1029/2012JB009230

Ghosh, A., Huesca-Pérez, E., Brodsky, E., & Ito, Y. (2015). Very low frequency earthquakes in Cascadia migrate with tremor. *Geophysical Research Letters*, *42*(9), 3228–3232. https://doi.org/10.1002/2015GL063286

Hayes, G. (2018). Slab2 - A Comprehensive Subduction Zone Geometry Model, U.S. Geological Survey data release, https://doi.org/10.5066/F7PV6JNV

Helffrich, G., Wookey, J., & Bastow, I. (2013). The Seismic Analysis Code. Cambridge: Cambridge University Press. https://doi.org/10.1017/CBO9781139547260

Ide, S. (2016). Characteristics of slow earthquakes in the very low frequency band: Application to the Cascadia subduction zone, *Journal of Geophysical Research; Solid Earth*, 121, 5942–5952. https://doi.org/10.1002/2016JB013085

Ide, S., & Maury, J. (2018). Seismic Moment, Seismic Energy, and Source Duration of Slow Earthquakes: Application of Brownian slow earthquake model to three major subduction zones. *Geophysical Research Letters*, *45*(7), 3059–3067. https://doi.org/10.1002/2018GL077461

Ide, S., and Yabe, S. (2014). Universality of slow earthquakes in the very low frequency band, *Geophysical Research Letters*, 41, 2786–2793, https://doi.org/10.1002/2014GL059712

Ide, S., Imanishi, K., Yoshida, Y., Beroza, G. C., & Shelly, D. R. (2008). Bridging the gap between seismically and geodetically detected slow earthquakes. *Geophysical Research Letters*, *35*(10), 2–7. https://doi.org/10.1029/2008GL034014

Ito, Y., & Obara, K. (2006). Very low frequency earthquakes within accretionary prisms are very low stress-drop earthquakes. *Geophysical Research Letters*, *33*(9), 1–4. https://doi.org/10.1029/2006GL025883

Ito, Y., Obara, K., Shiomi, K., Sekine, S., & Hirose, H. (2007). Slow earthquakes coincident with episodic tremors and slow slip events. *Science*, 315(5811), 503–506. https://doi.org/10.1126/science.1134454

Ito, Y., Hino, R., Kido, M., Fujimoto, H., Osada, Y., Inazu, D., et al. (2013). Episodic slow slip events in the Japan subduction zone before the 2011 Tohoku-Oki earthquake. *Tectonophysics*, *600*, 14–26. https://doi.org/10.1016/j.tecto.2012.08.022

Jiang, Y., Wdowinski, S., Dixon, T. H., Hackl, M., Protti, M., & Gonzalez, V. (2012). Slow slip events in Costa Rica detected by continuous GPS observations, 2002-2011. *Geochemistry, Geophysics, Geosystems*, *13*(1), 1–18. https://doi.org/10.1029/2012GC004058

Jiang, Y., Liu, Z., Davis, E. E., Schwartz, S. Y., Dixon, T. H., Voss, N., et al. (2017). Strain release at the trench during shallow slow slip: The example of Nicoya Peninsula, Costa Rica. *Geophysical Research Letters*, *44*(10), 4846–4854. https://doi.org/10.1002/2017GL072803

Kanamori, H., & Rivera, L. (2006). Energy partitioning during an earthquake. *Geophysical Monograph Series*, *170*, 3–13. https://doi.org/10.1029/170GM03

Kato, A., & Nakagawa, S. (2014). Geophysical Research Letters. *Geophysical Research Letters*, (April), 6413–6419. https://doi.org/10.1002/2014GL061184.Received

Kato, A., Obara, K., Igarashi, T., Tsuruoka, H., Nakagawa, S., & Hirata, N. (2012). Propagation of slow slip leading up to the 2011 Mw 9.0 Tohoku-Oki earthquake, *Science*, 335, 705–708, https://doi.org/10.1126/science.1215141

Laske, G., Masters., G., Ma, Z., & Pasyanos, M. (2013). *Update on CRUST1.0 - A 1-degree Global Model of Earth's Crust*, Paper presented at EGU General Assembly, European Geoscience Union, Vienna

Maeda, T., & Obara, K. (2009). Spatiotemporal distribution of seismic energy radiation from low-frequency tremor in western Shikoku, Japan. *Journal of Geophysical Research: Solid Earth*, *114*(10). https://doi.org/10.1029/2008JB006043

Maeda, T., Takemura, S., & Furumura, T. (2017). OpenSWPC: An open-source integrated parallel simulation code for modeling seismic wave propagation in 3D heterogeneous

viscoelastic media 4. Seismology. *Earth, Planets and Space*, *69*(1). https://doi.org/10.1186/s40623-017-0687-2

Nakano, M., Hori, T., Araki, E., Kodaira, S., & Ide, S. (2018). Shallow very-low-frequency earthquakes accompany slow slip events in the Nankai subduction zone /704/2151/210 /704/2151/508 article. *Nature Communications*, *9*(1). https://doi.org/10.1038/s41467-018-03431-5

Nishikawa, T., Matsuzawa, T., Ohta, K., Uchida, N., Nishimura, T., & Ide, S. (2019). The slow earthquake spectrum in the Japan Trench illuminated by the S-net seafloor observatories. *Science (New York, N.Y.)*, *365*(6455), 808–813. https://doi.org/10.1126/science.aax5618

Obara, K. (2002). Nonvolcanic deep tremor associated with subduction in southwest Japan. Science, 296(5573), 1679–1681. https://doi.org/10.1126/science.1070378

Obara, K. (2011). Characteristics and interactions between non-volcanic tremor and related slow earthquakes in the Nankai subduction zone, southwest Japan. *Journal of Geodynamics*, *52*(3–4), 229–248. https://doi.org/10.1016/j.jog.2011.04.002

Obara, K., & Ito, Y. (2005). Very low frequency earthquakes excited by the 2004 off Kii peninsula earthquakes: A dynamic deformation process in the large accretionary prism. *Earth, Planets and Space*, *57*(4), 321–326. https://doi.org/10.1186/BF03352570

Obara, K., & Kato, A. (2016). Connecting slow earthquakes to huge earthquakes. *Science (New York, N.Y.)*, *353*(6296), 253–257. https://doi.org/10.1126/science.aaf1512

Outerbridge, K. C., Dixon, T. H., Schwartz, S. Y., Walter, J. I., Protti, M., Gonzalez, V., et al. (2010). A tremor and slip event on the Cocos-Caribbean subduction zone as measured by a global positioning system (GPS) and seismic network on the Nicoya Peninsula, Costa Rica. *Journal of Geophysical Research: Solid Earth*, *115*(10), 1–17. https://doi.org/10.1029/2009JB006845

Rogers, G., & Dragert, H. (2003). Episodic tremor and slip on the Cascadia subduction zone: The chatter of silent slip. *Science*, 300(5627), 1942–1943. https://doi.org/10.1126/science.1084783

Rost, S., and Thomas, C. (2002), Array seismology: Methods and applications, *Reviews of Geophysics,* 40, 3. https://doi.org/10.1029/2000RG000100

Protti, M. (1995). The March 25, 1990 (Mw=7.0, ML=6.8), earthquake at the entrance of the Nicoya Gulf, Costa Rica: its prior activity, foreshocks, aftershocks, and triggered seismicity. *Journal of Geophysical Research*, *100*(B10), 345–358. https://doi.org/10.1029/94jb03099

Protti, Marino, González, V., Newman, A. V., Dixon, T. H., Schwartz, S. Y., Marshall, J. S., et al. (2014). Nicoya earthquake rupture anticipated by geodetic measurement of the locked plate interface. *Nature Geoscience*, *7*(2), 117–121. https://doi.org/10.1038/ngeo2038

Ruiz S., Aden-Antoniow F., Baez, J. C., Otarola, C., Potin, B., Campo, F., Poli, P., Flores, C., Satriano, C., Leyton, F., Madariaga, R., Bernard, P. (2017). Nucleation phase and dynamic inversion of the Mw 6.9 Valparaíso 2017 earthquake in Central Chile. Geophysical Research Letters, 44, 10290–10297. https://doi.org/10.1002/2017GL075675

Satake, K. (1994). Mechanism of the 1992 Nicaragua Tsunami Earthquake. *Geophysical Research Letters*, *21*(23), 2519–2522. https://doi.org/10.1029/94GL02338

Sato, H., Fehler, M., & Maeda, T. (2012). *Seismic Wave Propagation and Scattering in the Heterogeneous Earth Structure, 2nd ed.*, New York, Springer-Verlag.

Scripps Institution of Oceanography. (1986). IRIS/IDA Seismic Network. International Federation of Digital Seismograph Networks. https://doi.org/10.7914/SN/II

620 Shelly, D. R., Beroza, G. C., Ide, S., & Nakamula, S. (2006). Low-frequency earthquakes in
621 Shikoku, Japan, and their relationship to episodic tremor and slip. *Nature*, *442*(7099), 188–
622 191. https://doi.org/10.1038/nature04931
623 Shelly, D. R., Beroza, G. C., & Ide, S. (2007). Non-volcanic tremor and low-frequency
624 earthquake swarms. *Nature*, *446*(7133), 305–307. https://doi.org/10.1038/nature05666
625 Shipley, T. H., Stoffa, P. L., & Dean, D. F. (1990). Underthrust sediments, fluid migration paths,
626 and mud volcanoes associated with the accretionary wedge off Costa Rica: Middle America
627 Trench. *Journal of Geophysical Research*, 95(B6), 8743–8752.
628 https://doi.org/10.1029/JB095iB06p08743
629 Solomon, E. A., Kastner, M., Wheat, C. G., Jannasch, H., Robertson, G., Davis, E. E., & Morris,
630 J. D. (2009). Long-term hydrogeochemical records in the oceanic basement and forearc
631 prism at the Costa Rica subduction zone. *Earth and Planetary Science Letters*, *282*(1–4),
632 240–251. https://doi.org/10.1016/j.epsl.2009.03.022
633 Sugioka, H., Okamoto, T., Nakamura, T., Ishihara, Y., Ito, A., Obana, K., et al. (2012).
634 Tsunamigenic potential of the shallow subduction plate boundary inferred from slow
635 seismic slip. *Nature Geoscience*, *5*(6), 414–418. https://doi.org/10.1038/ngeo1466
636 Syracuse, E. M., van Keken, P. E., Abers, G. A., Suetsugu, D., Bina, C., Inoue, T., et al. (2010).
637 The global range of subduction zone thermal models. *Physics of the Earth and Planetary*
638 *Interiors*, *183*(1–2), 73–90. https://doi.org/10.1016/j.pepi.2010.02.004
639 Takagi, R., Uchida, N., & Obara, K. (2019). Along-Strike Variation and Migration of Long-
640 Term Slow Slip Events in the Western Nankai Subduction Zone, Japan. *Journal of*
641 *Geophysical Research: Solid Earth*, (Figure 1), 3853–3880.
642 https://doi.org/10.1029/2018JB016738
643 Takemura, S., Kobayashi, M., & Yoshimoto, K. (2017). High-frequency seismic wave
644 propagation within the heterogeneous crust: Effects of seismic scattering and intrinsic
645 attenuation on ground motion modelling. *Geophysical Journal International*, *210*(3), 1806–
646 1822. https://doi.org/10.1093/gji/ggx269
647 Takemura, S., Matsuzawa, T., Noda, A., Tonegawa, T., Asano, Y., Kimura, T., & Shiomi, K.
648 (2019). Structural Characteristics of the Nankai Trough Shallow Plate Boundary Inferred
649 From Shallow Very Low Frequency Earthquakes. *Geophysical Research Letters*, *46*(8),
650 4192–4201. https://doi.org/10.1029/2019GL082448
651 Takemura, S., Okuwaki, R., Kubota, T., Shiomi, K., Kimura, T., & Noda, A. (2020). Centroid
652 moment tensor inversions of offshore earthquakes using a three-dimensional velocity
653 structure model: slip distributions on the plate boundary along the Nankai Trough.
654 *Geophysical Journal International*, *222*(2), 1109–1125. https://doi.org/10.1093/gji/ggaa238
655 Tamaribuchi, K., Kobayashi, A., Nishimiya, T., Hirose, F., & Annoura, S. (2019).
656 Characteristics of Shallow Low-Frequency Earthquakes off the Kii Peninsula, Japan, in
657 2004 Revealed by Ocean Bottom Seismometers. *Geophysical Research Letters*, *46*(23),
658 13737–13745. https://doi.org/10.1029/2019GL085158
659 Tonegawa, T., Araki, E., Kimura, T., Nakamura, T., Nakano, M., & Suzuki, K. (2017). Sporadic
660 low-velocity volumes spatially correlate with shallow very low frequency earthquake
661 clusters. *Nature Communications*, *8*(1), 2048. https://doi.org/10.1038/s41467-017-02276-8
662 Uchida, N., & Matsuzawa, T. (2013). Pre- and postseismic slow slip surrounding the 2011
663 Tohoku-oki earthquake rupture. *Earth and Planetary Science Letters*, *374*, 81–91.
664 https://doi.org/10.1016/j.epsl.2013.05.021

Voss, N., Dixon, T. H., Liu, Z., Malservisi, R., Protti, M., & Schwartz, S. (2018). Do slow slip events trigger large and great megathrust earthquakes? *Science Advances*, *4*(10), 1–6. https://doi.org/10.1126/sciadv.aat8472

Walter, J. I., Schwartz, S. Y., Protti, J. M., & Gonzalez, V. (2011). Persistent tremor within the northern Costa Rica seismogenic zone. *Geophysical Research Letters*, *38*(1), 1–5. https://doi.org/10.1029/2010GL045586

Walter, J. I., Schwartz, S. Y., Protti, M., & Gonzalez, V. (2013). The synchronous occurrence of shallow tremor and very low frequency earthquakes offshore of the Nicoya Peninsula, Costa Rica. *Geophysical Research Letters*, *40*(8), 1517–1522. https://doi.org/10.1002/grl.50213

Wessel, P., Smith, W. H. F., Scharroo, R., Luis, J., & Wobbe, F. (2013). Generic mapping tools: Improved version released. Eos, Transactions American Geophysical Union, 94(45), 409–410. https://doi.org/10.1002/2013EO450001

Yabe, S., Nakano, M., Tonegawa, T., Baba, S., & Takemura. S. (2020). *Seismic energy estimation for shallow tremors in the Nankai trough and Japan trench*, Paper presented at JpGU-AGU Joint Meeting 2020: Virtual, Japan Geoscience Union & American Geophysical Union, Online

Yabe, S., Tonegawa, T., & Nakano, M. (2019). Scaled Energy Estimation for Shallow Slow Earthquakes. *Journal of Geophysical Research: Solid Earth*, *124*(2), 1507–1519. https://doi.org/10.1029/2018JB016815

Yao, S., & Yang, H. (2020). Rupture Dynamics of the 2012 Nicoya Mw 7.6 Earthquake: Evidence for Low Strength on the Megathrust. *Geophysical Research Letters*, *47*(13), 1–11. https://doi.org/10.1029/2020GL087508

Yoshimoto, K., Sato, H., & Ohtake, M. (1993). Frequency-Dependent Attenuation of P and S Waves In the Kanto Area, Japan, Based On the Coda-Normalization Method. *Geophysical Journal International*, *114*(1), 165–174. https://doi.org/10.1111/j.1365-246X.1993.tb01476.x

Yue, H., Lay, T., Schwartz, S. Y., Rivera, L., Protti, M., Dixon, T. H., et al. (2013). The 5 September 2012 Nicoya, Costa Rica Mw 7.6 earthquake rupture process from joint inversion of high-rate GPS, strong-motion, and teleseismic P wave data and its relationship to adjacent plate boundary interface properties. *Journal of Geophysical Research: Solid Earth*, *118*(10), 5453–5466. https://doi.org/10.1002/jgrb.50379